Network dynamics of chalcogenide glasses. II. Silicon diselenide

M. Arai,* D. L. Price, S. Susman, K. J. Volin, and U. Walter†
Materials Science Division and Intense Pulsed Neutron Source, Argonne National Laboratory, Argonne, Illinois 60439-4843
(Received 6 July 1987)

The scattering function $S(Q,E)$ of vitreous $SiSe_2$ at 50 K was measured with inelastic neutron scattering over a wide range of variables ($0.5 < Q < 12$ Å^{-1}, $-20 < E < 80$ meV), with use of a chopper spectrometer at the Intense Pulsed Neutron Source. The data are analyzed in terms of the effective one-phonon density of states $G(E)$, the Q dependence of $S(Q,E)$ at different values of energy transfer E, and the elastic structure factor $S_{el}(Q)$. The data are discussed in terms of the normal modes of vibration of a $Si(Se_{1/2})_4$ molecule. Certain features in the data can be generally identified with such modes on the basis of the behavior of the dynamic structure factor $S(Q,E)$ at fixed E. Other features imply more complex structural entities, including edge-linked tetrahedral chains characteristic of crystalline $SiSe_2$ and an admixture of corner-sharing units, not found in the crystal.

I. INTRODUCTION

Vitreous silicon diselenide, while less extensively studied than its germanium analogue, is a stable glass that can be prepared by melt-quenching techniques. Among the other members of the Si_xSe_{1-x} series of glasses, the $SiSe_2$ composition is characterized by a maximum in the molar volume and in the glass transition temperature as a function of x.[1] The structure of the crystalline form of $SiSe_2$ has been measured by x-ray diffraction:[2] it comprises chains of edge-bonded $Si(Se_{1/2})_4$ tetrahedra, in contrast to crystalline $GeSe_2$ in which edge sharing and corner sharing of $Ge(Se_{1/2})_4$ tetrahedra both occur.[3] An extensive series of neutron diffraction measurements[4] carried out at Argonne National Laboratory on Si_xSe_{1-x} glasses indicate that the tetrahedra are predominantly edge sharing in the glass as well, although Raman scattering data[5–8] suggest some admixture of corner sharing. A recent computer-generated model of Gladden and Elliott[9] infers 15% of corner-shared units from the diffraction data of Ref. 4. Both corner sharing and edge sharing appear to be significant in Ge_xSe_{1-x} glasses (preceding paper,[10] henceforth cited as I, and references therein). There is considerable interest, therefore, in examining the network dynamics of vitreous $SiSe_2$ and in making comparison with results from similar studies on $GeSe_2$ (Ref. 10) and also on SiO_2,[11] for which there are firm grounds for believing that the structure is composed purely of corner-shared $Si(O_{1/2})_4$ tetrahedra.

II. EXPERIMENTAL PROCEDURES

The formalism of the inelastic neutron scattering technique is described in I; we will refer to the formulas given there where necessary. In this section we will discuss only those aspects of the $SiSe_2$ measurements which differ from those described for $GeSe_2$.

A. Sample preparation

The preparation of pure silicon diselenide glass requires attention to detail. $SiSe_2$ is a line compound with a melting point of 960 °C. It is the only congruently melting composition within the Se-rich region of the phase diagram.[1] In the vitreous phase it is a moderately reactive solid that hydrolyzes and decomposes rapidly upon exposure to the room environment. Elemental silicon and selenium are far less reactive, but in the synthesis of g-$SiSe_2$ they can serve as sources of oxygen and hydrogen contamination. However, the fused silica ampoule that is used to contain the $SiSe_2$ melt is not easily replaced by a different container material. This section contains a brief description of the procedure used for preparing pure samples of the size ($\simeq 60$ g) required for inelastic neutron scattering. A full description is presented elsewhere.[12]

The glass transition temperature of g-$SiSe_2$ is 424 °C and the crystallization temperature is 575 °C.[1] Conventional quenching of $Si_{0.33}Se_{0.67}$ melts in 10–13-mm-o.d. silica tubes results in a largely crystalline product. Even with accelerated quenching at 500 K/sec,[4] the stoichiometric glass melt solidifies into a cylindrical boule with only a 2-mm annular ring of glass and a core of crystalline $SiSe_2$. Bulk samples of the glass have been conveniently prepared by moving slightly away from stoichiometry to compositions $Si_{0.34}Se_{0.66}$ or $Si_{0.32}Se_{0.68}$. For the purposes of inelastic neutron scattering, this departure from stoichiometry is not significant and, in this paper, the glass will be labeled g-$SiSe_2$.

Semiconductor-grade, O-free (<0.2 ppm) silicon lump was pulverized in a helium-purged glove box. Stoichiometric proportions were combined with 99.9995% pure selenium which had been further treated to remove surface oxide.[12] Twenty-gram batches were loaded onto pretreated, 10-mm-o.d. fused silica tubes. The melts were homogenized at 1100–1140 °C in a rocking furnace and the vacuum-sealed ampoules were quenched into a 10% NaOH-H_2O bath. The resultant

$SiSe_2$ glass samples were extensively characterized for stoichiometry, purity, crystallinity, and homogeneity by chemical analyses, Raman scattering, ir absorption spectrometry, and optical microscopy. If samples are not mounted in evacuated cells or cryostats and handled carefully, they immediately pick up a chemisorbed surface layer of H_2O as revealed by the 1695-cm^{-1} H—O—H bending mode.

B. Neutron measurements

Inelastic neutron scattering measurements were made by time-of-flight technique, principally on the low-resolution medium-energy chopper spectrometer[13] at the Intense Pulsed Neutron Source, Argonne National Laboratory. The vitreous $SiSe_2$ sample was mounted in a special aluminum container in order to avoid reaction with atmospheric moisture. A sample temperature of $\simeq 50$ K was maintained in a Displex refrigerator. The sample was made up of small pieces of glass with a total weight of 60 g and approximate dimensions of 6.4 cm high $\times 7.6$ cm wide $\times 0.376$ cm thick. It was mounted in transmission geometry at an angle of 45° to the incident beam, giving a transmission of 0.841. The incident neutron energy was 101.6 meV, measured from the time-of-flight spectra in beam monitors up- and downstream from the sample. The scattered neutron spectra recorded in 36 detector groups covering scattering angles ϕ from 2.6° to 107.4° gave $S(Q,E)$ [see Eq. (1) of I] for a Q range from 0.5 to 12 $Å^{-1}$ (at $E=0$, smaller for $E>0$) and an E range from -20 to $+80$ meV. As in the case of $GeSe_2$, the scattering function is dominated by the coherent part $S_c(Q,E)$, Eq. (2) of I. Runs were made with the $SiSe_2$ sample (55 h), the empty Al container (47 h), a vanadium standard (6 h), and an empty sample holder (5 h); the purpose of the last two runs was to calibrate the different detector groups.

In order to obtain higher-resolution information about the density of states, a second measurement was made on the high-resolution medium-energy chopper spectrometer (HRMECS)[13] using the newly installed high-angle detector banks at $\phi=86.9°$, 105.9°, 120.9°, and 136.2°. Since this data set included only these four angles, it was not possible to study the Q dependence; however, more accurate information about the density of states was obtained, especially for the region below 50 meV. The incident energy (96.7 meV) and sample size (61.4 g) were similar to those of the LRMECS measurement; the sample was spread out over a larger area, however, giving a higher transmission (0.888). The sample temperature in this measurement was 13 K, somewhat lower than that of the earlier experiment. The difference is not expected to be significant in this material.

C. Data analysis

The data were analyzed using standard routines.[14] A correction to the LRMECS data for multiple scattering was made using the Monte Carlo program MSCAT.[15] The kernel consisted of an elastic scattering component, based on the values for the static structure factor $S(Q)$ measured in Ref. 4, and an inelastic component based on the incoherent approximation[10,11] using an initial estimate for the effective density of states $G(E)$ (see Sec. III B below). The Monte Carlo simulation was run for 80 000 neutrons. The measured values of $S(\phi,E)$ were then corrected for the effects of multiple scattering and of self-shielding within the sample. A final intensity normalization (required because of uncertainty in the volume of sample in the beam) was made so that $S(Q)$ derived from the corrected $S(\phi,E)$ data agreed with the diffraction data of Ref. 4 (see below). Figure 1 shows an example of the data before the correction and the multiple and single scatterings calculated within the simulation. The $S(\phi,E)$ data were then interpolated onto constant Q to provide $S(Q,E)$ over the (Q,E) range of the measurement: $0.5<Q<12$ $Å^{-1}$ (at $E=0$) and $-20<E<80$ meV.

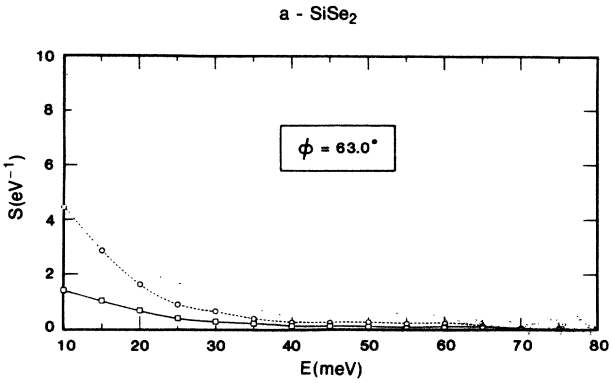

FIG. 1. Example of the experimental data for $S(Q,E)$ at a scattering angle $\phi=63.0°$. The solid and dashed lines show the multiple and single scatterings calculated in the Monte Carlo simulation of the experiment described in the text. The dotted line shows the uncorrected data.

The HRMECS data were left in the $S(\phi,E)$ form because interpolation was not appropriate in view of the limited range of detector angles. These data were also not corrected for multiple-scattering or self-shielding effects in view of their more limited application.

III. RESULTS AND DISCUSSION

A. Total and elastic scattering

Figure 2 shows a comparison between the values of $S(Q)$ obtained from the LRMECS measurements by integration of $S(Q,E)$ over the measured range of E (-20 to 80 meV) and those obtained in Ref. 4 from diffraction measurements. The latter have been corrected to allow for the small amount of incoherent scattering from Se. The agreement is seen to be satisfactory. The values from the inelastic data fall off at high Q because the energy range begins to be restricted by kinematic effects and so the higher E part of $S(Q,E)$ is excluded from the integral. Also, the peaks at lower Q are broader in the inelastic data because of poorer Q resolution (about 0.3 $Å^{-1}$ compared with 0.09 $Å^{-1}$ in the diffraction experiment).

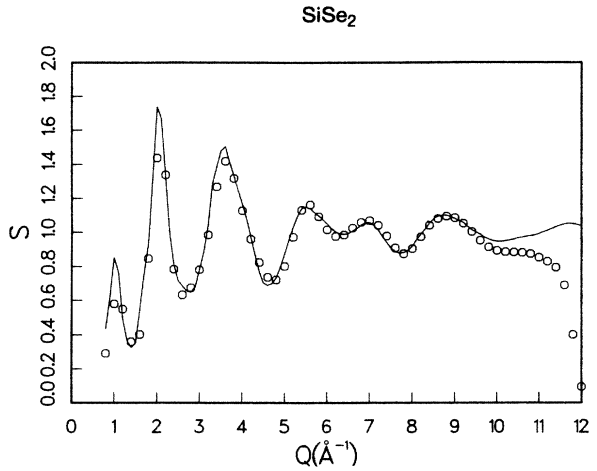

FIG. 2. $S(Q)$ derived from integration of $S(Q,E)$ from this experiment (○) with that measured in a diffraction experiment (Ref. 7) (——).

The elastic scattering was estimated by fitting a Gaussian peak superimposed on a smooth background at each value of Q. This procedure is not strictly valid because the energy resolution is an asymmetric function reflecting the shape of the source pulse.[16] Nevertheless it appears to do a reasonable job of estimating the elastic scattering in the case of incident neutron energies of 100 meV and above. The fitted intensities were used to estimate $S_{el}(Q)$. Figure 3 shows a plot of the functions $\ln[S_{el}(Q)/S(Q)]$ and $\ln[S_{el}(Q)-S(Q)+1]$; the latter is expected[10,11] to approach the mean Debye-Waller factor defined in Eq. (13) of I in the limiting case where there is negligible correlation in the thermal motions of neighboring atoms. Figure 3 suggests that this condition is reasonably well met, and that the mean Debye-Waller factor can be roughly approximated by $\exp(-\alpha Q^2)$ with $\alpha=0.002\,57$ Å^2.

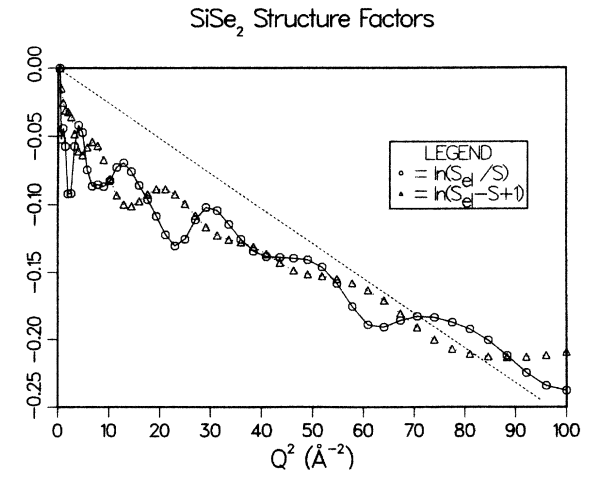

FIG. 3. Structure factors for $SiSe_2$ plotted against Q^2: $\ln[S_{el}(Q)/S(Q)]$ (——); $\ln[S_{el}(Q)-S(Q)+1]$ (· · · ·); and $(-\alpha Q^2)$ with $\alpha=0.002\,57$ Å^2 (— — —).

B. Density of states

The effective density of states was obtained by averaging $G(Q,E)$, derived from the LRMECS $S(Q,E)$ data by use of Eqs. (9) and (10) of I and $\langle \overline{u^2} \rangle/3=0.00257$ Å^2, over the range $4.5<Q<11$ Å^{-1}. The result, corrected for multiphonon scattering using the procedure described in Ref. 10, is shown in Fig. 4. The spectrum is characterized by a broad peak in the region of 12 meV (97 cm^{-1}), followed by three peaks at a higher energy centered approximately at 29, 47, and 58.5 meV (234, 379, and 472 cm^{-1}). (The conversion 1 meV = 8.0655 cm^{-1} is used.) In addition, there is the suggestion of a shoulder at around 64 meV (516 cm^{-1}) on the side of the highest-energy peak.

An analogous effective density of states was obtained from the HRMECS $S(\phi,E)$ data by averaging the constant-ϕ data for the four detector banks and is shown in Fig. 5. The multiphonon component has again been subtracted. The agreement for the general shape of the densities of states from the two measurements is quite satisfactory. However, with the higher resolution of the HRMECS experiment [3 meV full width at half maximum (FWHM) compared with about 6 meV in the LRMECS measurement], it was possible to resolve additional features. The broad peak at 12 meV now reveals considerable structure, with at least two peaks, approximately centered at 6 and 14 meV (48 and 113 cm^{-1}), and possibly a third at an intermediate value around 10 meV (81 cm^{-1}). The 29-meV peak now appears as a doublet with peak energies of 27 and 30 meV (218 and 242 cm^{-1}), the 47-meV peak is resolved into a doublet with peak energies 45.5 and 49.5 meV (367 and 399 cm^{-1}), and a new feature can be distinguished at 37.5 meV (302 cm^{-1}). The features in the LRMECS data at 58.5 and 64 meV are not clearly expressed in the HRMECS data because of the poor statistics at high energy transfer. For the listing of the neutron peak energies given in Table I, the LRMECS values are used for the last two features and

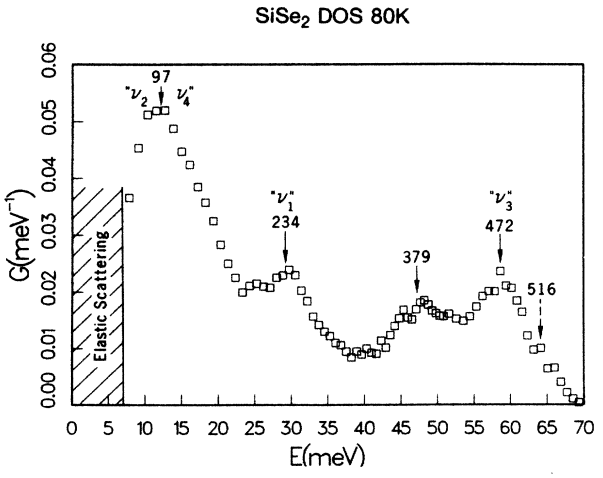

FIG. 4. One-phonon effective density of states $G(E)$ from the LRMECS measurement; the labels attached to features in $G(E)$ give the frequency in cm^{-1} and, where appropriate, assignments discussed in the text in terms of modes of an $Si(Se_{1/2})_4$ tetrahedron.

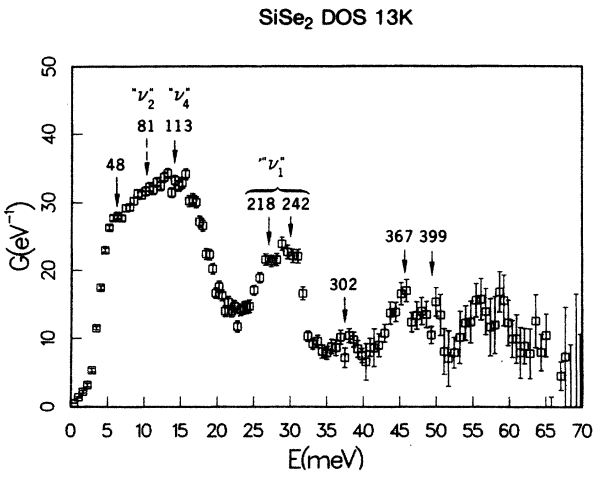

FIG. 5. Same as Fig. 4, with data from HRMECS.

the HRMECS values for all the preceding ones.

Table I compares the energies of the neutron peaks with those observed in some of the Raman (Refs. 5–8) and ir (Ref. 8) measurements in the literature. The entries in a given row simply represent peaks observed in a similar energy interval, which may or may not represent the same physical feature. The assignments given by the different authors are shown in the right-hand part of the table.

As discussed in Sec. I, $SiSe_2$ is believed to consist of $Si(Se_{1/2})_4$ tetrahedra; the fraction of homopolar bonds, required for other types of structure, appears to be $<1\%$.[4] A model based on isolated tetrahedra should therefore provide a reasonable starting point for discussing the dynamics of the glass. In the Sen-Thorpe picture, discussed in Sec. III B of I in connection with $GeSe_2$, the value of the critical bond angle θ_c is imaginary for $SiSe_2$, and so the isolated tetrahedral model is appropriate for any value of the bond angle θ. This makes the density of states appear very different from that in SiO_2, where $\theta > \theta_c$ and the $O(Si_{1/4})_2$ unit provides a more suitable starting point.[11] The sixth column of Table I shows the four fundamental frequencies of the closest tetrahedral molecule, $SiBr_4$.[17] As in the case of $GeSe_2$, modes close to the molecular frequencies are observed in both crystalline and amorphous $SiSe_2$,[7,8] and can be assigned to the general character of the molecular frequencies with reasonable confidence. However, it is clear that the dynamics of the glass are more complicated than this simple picture allows: recent Raman measurements[5–7] identify four optical peaks in the region of the $\nu_1(A_1)$ tetrahedral vibrations (210–250 cm^{-1}) and at least four more in the region of the $\nu_3(F_2)$ vibration (350–520 cm^{-1}).

Griffiths *et al.*[7] and Tenhover *et al.*[8] have attempted to interpret the Raman spectrum of $SiSe_2$ glass by drawing an analogy to the spectrum of the crystal. Orthorhombic $SiSe_2$ is made up of chains of edge-sharing $Si(Se_{1/2})_4$ tetrahedra. This analysis reveals 15 optical modes, or which nine are Raman active and five ir active. None is both Raman and ir active. The authors proceeded to identify features of the optical spectra of both crystalline and vitreous material with these modes, as indicated in columns 9 and 10 of Table I. On the basis of the atomic displacements in these modes, one (A_g) could be associated with the $\nu_2(E)$ tetrahedral mode, two (B_{2g},B_{3g}) with the $\nu_4(F_2)$ tetrahedral mode, two more (B_{1g}, A_g) with the $\nu_1(A_1)$ mode, and six modes, three Raman active (B_{3g},B_{2g},B_{1g}) and three ir active (B_{2u},B_{3u},B_{1u}), with the $\nu_3(F_2)$ tetrahedral mode. These modes may be sufficient to account for the features observed in crystalline $SiSe_2$, but even this cannot be evaluated critically without accurate depolarization ratio measurements. The analogy breaks down for the glass in significant ways. The assignment of the Raman feature at 70 cm^{-1} to the $\nu_2(E)$ tetrahedral mode requires A_g symmetry. However, Susman *et al.*[5] have obtained accurate polarized Raman spectra and have shown that this mode is unpolarized. The $\nu_1(A_1)$ region of the spectrum remains an enigma since only two of the crystalline

TABLE I. Neutron and optical peaks in density of states of *a*-$SiSe_2$. (Question marks indicate uncertain values.)

Neutron (Present work)	Measured frequencies (cm^{-1}) Raman/ir (Ref. 5)	(Ref. 6)	(Ref. 7)	(Ref. 8)	$SiBr_4$ (Ref. 17)	Assignment[a] $SiSe_2$ (Ref. 5)	(Ref. 6)	(Ref. 7)	(Ref. 8)	$SiBr_4$ (Ref. 17)
48										
81	70		70	68	90	ES		A_g	A_g	$\nu_2(E)$
113	125		131	$\simeq$110	137				B_{2g},B_{3g}	$\nu_4(F_2)$
218	213	213	202	216		A_1	A_1	B_{1g}	B_{1g}	
	219	222	218			A_1^*	A_1	CS		
242	237	240	236	242	249	A_1	A_1^*	CS	A_g	
	245	248	245			A_1^*	A_1^*	A_g		
302	307		303							
367	357		358	350		ES		B_{3g}	B_{2g},B_{3g}	
399	387		380	390 (ir)				B_{2g}	B_{2u}	
472	470		470	460 (ir)	487			CS	B_{1u}	$\nu_3(F_2)$
				490 (ir)					B_{3u}	
516?	515		521	515				B_{1g}	B_{1g}	

[a]Symbols other than conventional symmetry designations have the following meaning: A_1^*: A_1 mode of edge-sharing tetrahedra; CS: corner-sharing tetrahedra; ES: edge-sharing tetrahedra.

modes appear in this region compared with the four observed in the Raman spectra, and all four are highly polarized.[5]

A possible solution to this discrepancy was suggested by Griffiths *et al.*,[7] based on the possible occurrence of corner-sharing tetrahedra in the glass, which are absent in the crystal. A minority component of such entities is consistent with the diffraction data.[4,9] Sugai[6] has advanced a stochastic model for the concentration of these entities as a function of composition for several chalcogenide glasses. For $SiSe_2$, assigning the 213- and 222-cm^{-1} Raman peaks to the A_1 (corner-sharing) and the 240- and 248-cm^{-1} Raman peaks to the A_1^* (edge-sharing) modes (he does not comment on why there are two of each), Sugai estimates 20–25 % of the Se atoms to be in corner-sharing configurations. It is to be noted that Refs. 5–7, while adopting a similar interpretation in terms of mixed corner and edge sharing, give three different assignments for the four modes.

The mode observed both in the Raman spectrum and in the HRMECS neutron spectrum around 305 cm^{-1} is also unaccounted for on the basis of the crystalline mode analysis. Griffiths *et al.* suggest an analogy with a mode found in $FSiBr_3$ molecules.

C. Dynamic structure factors

As demonstrated in I for the case of $GeSe_2$, the Q dependence of the scattering function at a given value of E provides, in principle, a means of identifying the features in the density of states observed at that energy. The calculations based on a tetrahedral model described in I were repeated with parameters appropriate for $SiSe_2$.

The values used for the force constants were $f_1'''=260$ and $f_2'''=27$ kdyn/cm, giving 67, 84, 236, and 532 cm^{-1} for ν_2, ν_4, ν_1, and ν_3, respectively. The structure factors are not very sensitive to the values of the forces, however. Figures 6–8 compare the calculated structure factors for the ν_4, ν_1, and ν_3 modes with the measured structure factors at $E=13.9$, 30.6, and 60.1 meV (112, 247, and 485 cm^{-1}), energies close to those of the features in the density of states ascribed to those modes (see Table I). The ν_2 mode was not included in this comparison since it is not adequately resolved from the elastic scattering; acoustic modes must also be contributing in this region. The agreement between calculated and measured structure factors seen in Figs. 6–8 is reasonable but not as impressive as in the case of $GeSe_2$, discussed in Sec. III C of I. There are probably two reasons for this: the statistical quality of the data is not as high in the $GeSe_2$ experiment (shorter run times and lower source flux at the time of the measurement), and the scattering is dominated to a greater extent by the Se atoms, which are probably more sensitive to the coupling of the tetrahedra than the group-IV atoms at the centers.

For completeness, Fig. 9 shows the structure factor measured at $E=48.2$ meV (389 cm^{-1}). This does not resemble the behavior calculated for the ν_3 tetrahedral mode as much as the structure factor measured at 485 cm^{-1} (Fig. 8), which supports the interpretation of the Raman peaks in this region in terms of modes of the $SiSe_2$

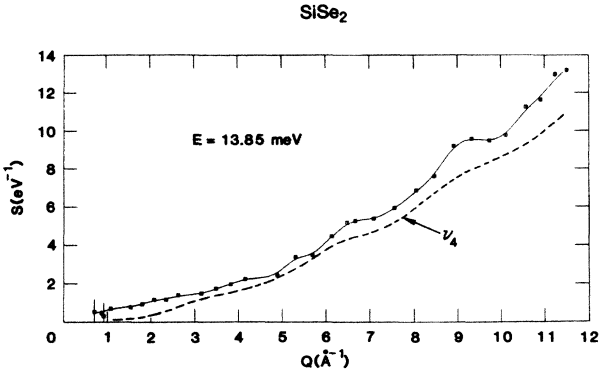

FIG. 6. The dynamic structure factor $S(Q,E)$ measured at 13.9 meV (□) (112 cm^{-1}); the solid line passing near the data points represents a smoothed cubic spline fit to the data. The curve marked ν_4 represents a calculation based on $Si(Se_{1/2})$ tetrahedra.

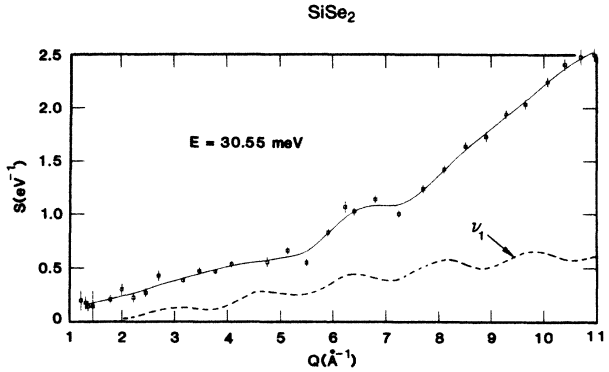

FIG. 7. $S(Q,E)$ measured at 30.6 meV (247 cm^{-1}); notation as for Fig. 6.

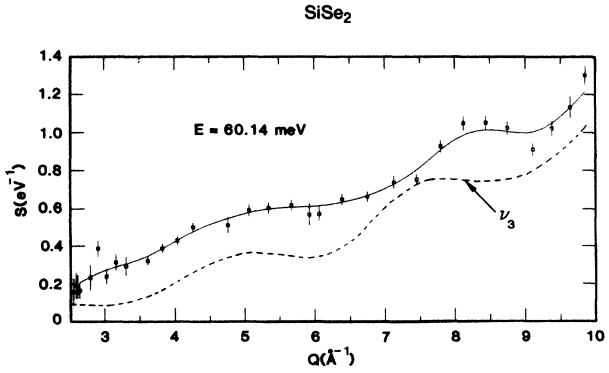

FIG. 8. $S(Q,E)$ measured at 60.1 meV (485 cm^{-1}); notation as for Fig. 6.

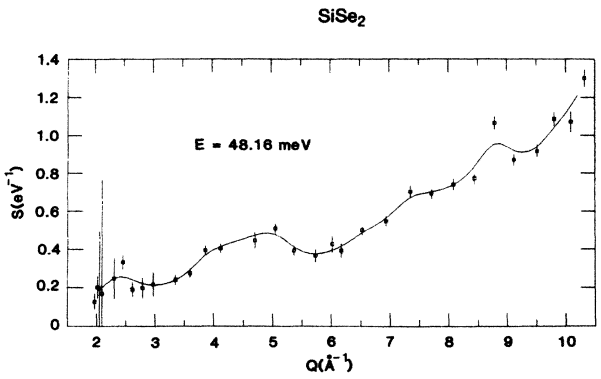

FIG. 9. $S(Q,E)$ measured at 48.2 meV (389 cm^{-1}).

(edge-sharing tetrahedra) crystal structure. It would be instructive to calculate the neutron structure factors for the fundamental unit of the crystalline structure, the analogue of the diborane molecule, but this has not been done in the present work. Additional insight into the nature of these modes may be provided by molecular-dynamics simulations now in progress at Argonne National Laboratory.[18]

Finally, the question arises as to whether a neutron structure factor analysis can shed light on questions such as the assignment of the four Raman modes observed in the $\nu_1(A_1)$ region and the identification of the 305-cm^{-1} mode. The answer is, in principle yes, but that such a determination would require a neutron spectrometer with resolution of 0.5 meV or better at 30-meV energy transfer and the angular range and intensity of LRMECS. Such capabilities probably do not exist anywhere at the present time, but may be hoped for in the new generation of spallation sources.

IV. CONCLUSIONS

The neutron inelastic studies reported in this work provide a picture of the dynamics of vitreous $SiSe_2$ that is generally consistent with that derived from optical measurements over the last ten years. Features associated with three of the four fundamental modes of the $Si(Se_{1/2})_4$ molecule can be identified in the one-phonon density of states, and are confirmed by a structure factor analysis; the lowest such mode overlaps the elastic and acoustic mode scattering. The data reveal two peaks in the region of the $\nu_1(A_1)$ tetrahedral mode compared with the four observed in high-resolution Raman scattering; they do not therefore settle the controversial assignments of these modes. It seems likely, however, that the multiplicity of these modes is due to a coexistence of edge and corner sharing of the $Si(Se_{1/2})_4$ tetrahedra. A peak observed in the Raman spectrum at 305 cm^{-1} appears clearly in the higher-resolution neutron data; its origin is not determined at the present time. Three and possibly four features are observed in the region of the $\nu_3(F_2)$ tetrahedral mode; these may reasonably be explained by vibrations of the edge-linked tetrahedral chain structure found in crystalline $SiSe_2$.

ACKNOWLEDGMENTS

The experimental measurements were carried out at the Intense Pulsed Neutron Source (IPNS) at Argonne National Laboratory, and the assistance of the IPNS Operations Staff is gratefully acknowledged. The authors have benefited from discussions with J. M. Carpenter, I. Ebbsjö, R. W. Johnson, R. Kalia, C.-K. Loong, T. I. Morrison, G. K. Shenoy, P. Vashishta, and A. C. Wright. This work was supported by the U.S. Department of Energy (Basic Energy Sciences Program, Division of Materials Sciences), under Contract No. W-31-109-ENG-38.

*Present address: National Laboratory for High-Energy Physics, Tsukuba, Ibaraki, Japan.

†Present address: Department of Physics, University of California, Berkeley, CA 94720.

[1]R. W. Johnson, S. Susman, J. McMillan, and K. J. Volin, Mater. Res. Bull. **21**, 41 (1986).

[2]J. Peters and B. Krebs, Acta Crystallogr. Sect. B **38**, 1270 (1982).

[3]Von G. Dittmar and H. Schäfer, Acta Crystallogr. Sect. B **32**, 2726 (1976).

[4]R. W. Johnson, S. Susman, and D. L. Price, J. Non-Cryst Solids **75**, 57 (1985); R. W. Johnson, D. L. Price, S. Susman, M. Arai, T. I. Morrison, and G. K. Shenoy, *ibid.* **83**, 251 (1986); R. W. Johnson, *ibid.* **88**, 366 (1986).

[5]S. Susman, R. W. Johnson, D. L. Price, and K. J. Volin, *Defects in Glasses,* Mater. Res. Soc. Symp. Proc. No. 61, edited by F. L. Galeener, D. L. Griscom, and M. L. Weber (MRS, Boston, 1986), p. 91.

[6]S. Sugai, Phys. Rev. B **35**, 1345 (1987); also contains a comprehensive list of references to previous work.

[7]J. E. Griffiths, M. Malyj, G. P. Espinosa, and J. P. Remeika, Phys. Rev. B **30**, 6978 (1984); M. Malyj, G. P. Espinosa, and J. E. Griffiths, *ibid.* **31**, 3672 (1985).

[8]M. Tenhover, M. A. Hazle, and R. J. Grasselli, Phys. Rev. Lett. **51**, 404 (1983); M. Tenhover, M. A. Hazle, R. K. Grasselli, and C. W. Tompson, Phys. Rev. B **28**, 4608 (1983); M. Tenhover, R. S. Henderson, D. Lukco, M. A. Hazle, and R. K. Grasselli, Solid State Commun. **51**, 455 (1984).

[9]L. F. Gladden and S. R. Elliott, Phys. Rev. Lett. **59**, 908 (1987).

[10]U. Walter, D. L. Price, S. Susman, and K. J. Volin, preceding paper, Phys. Rev. B **37**, 4232 (1988).

[11]J. M. Carpenter and D. L. Price, Phys. Rev. Lett. **54**, 441 (1985); D. L. Price and J. M. Carpenter, J. Non-Cryst. Solids **92**, 153 (1987).

[12]S. Susman and K. J. Volin (unpublished).

[13]D. L. Price, J. M. Carpenter, C. A. Pelizzari, S. K. Sinha, I. Bresof, and G. E. Ostrowski, Argonne National Laboratory, 1982, Report No. ANL-82-80 (unpublished), p. 207.

[14]C. K. Loong and D. L. Price (unpublished).

[15]J. R. D. Copley, Comp. Phys. Commun. **7**, 289 (1974); **9**, 59 (1975); **9**, 64 (1975); **21**, 431 (1981); J. R. D. Copley, P. Verkerk, A. A. Van Well, and H. Fredrikze, Comp. Phys. Commun. **40**, 337 (1986); D. L. Price (unpublished).

[16]C.-K. Loong, S. Ikeda, and J. M. Carpenter, Nucl. Instrum. Methods A **260**, 381 (1987).

[17]G. Herzberg, *Infrared and Raman Spectra of Polyatomic Molecules* (Van Nostrand, New York, 1945).

[18]P. Vashishta (private communication).